Publisher homepage: www.universepg.com, ISSN: 2707-4625 (Online) & 2707-4617 (Print)
https://doi.org/10.34104/ijmms.022.083093
International Journal of Material and Mathematical Sciences
Journal homepage: www.universepg.com/journal/ijmms

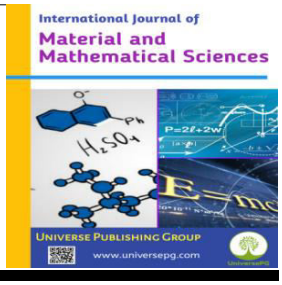

Synthesis a Clay Based Photocatalyst for the Removal of Eosin Yellow in Aqueous Solution

Debadas Halder[1&2], Md Nazrul Islam[2], M Mufazzal Hossain[3], Md Ataur Rahman[3], Rajib Samadder[2], and Mohammad Mostafizur Rahman[4]*

[1]Institute of Education and Research, University of Dhaka, Dhaka-1000, Bangladesh; [2]Department of Chemistry, Bangladesh University of Engineering and Technology, Dhaka-1000, Bangladesh; [3]Department of Chemistry, University of Dhaka, Dhaka-1000, Bangladesh; [4]Department of Chemistry, Jagannath University, Dhaka-1100, Bangladesh.

*Correspondence: mostafiz@chem.jnu.ac.bd (Dr. Mohammad Mostafizur Rahman, Professor, Department of Chemistry, Jagannath University, Dhaka-1100, Bangladesh).

ABSTRACT

Composite photocatalysts of clay and ZnO have been prepared using three different compositions and characterized by various techniques such as SEM, EDX, FTIR, and XRD. SEM micrographs in different magnifications revealed different morphology of composite particles rather than commercial ZnO and clay. The particle size of the prepared composite decreased with the increasing amount of clay and thus improves the catalyst surface area. EDX revealed that composite contains clay and ZnO only. According to FTIR spectrum data, when the ratios of clay to ZnO are 12:88 and 25:75, all the clay particles are completely covered. The shift in the peak position of XRD patterns indicates the molecular level interaction between clay and ZnO. The composite photocatalyst with a composition of clay: ZnO = 25:75 has the highest capability to eliminate Eosin Yellow (EY) by both adsorption and photodegradation among the tested composite photocatalysts. At this composition, the degrading rate of 0.2 g of material in a 2×10^{-5} M aqueous solution was around 44.48% EY. However, after 60 minutes of photodegradation using UV light, the entire elimination of dye, including adsorption and photodegradation, is around 68.32%. As the concentration of EY increased, the degradation rate of EY reduced. It was discovered that the consequences of HCO_3^-, CO_3^{2-}, Cl^-, NO_3^-, and SO_4^{2-} ions were deleterious to the photodegradation of EY. It was also discovered that the UV source was more effective than the visible source. An intense UV light causes EY to completely degrade.

Keywords: Photocatalyst, Photodegradation, Composite, Wastewater, Aqueous solution, and Eosin yellow.

INTRODUCTION:

As results of industry's fast expansion, water pollution is currently a severe global issue. Huge amounts of waste from many sectors, including those in textile, plastic, paper, and cosmetics, are dumped into ponds, rivers, and lakes, which gravely harms the ecology and causes water pollution (Alqadami *et al.*, 2016). An estimated 7×10^5 metric tons of dyes are produced annually, of which 12% are lost during production and other handling steps. By using industrial effluent, around 20% of them harm the environment (Samadder *et al.*, 2020). High-colored effluents from the dyeing industry have low biological oxygen demand (BOD) and high chemical oxygen demand (COD) (Nasr *et al.*, 2006). Disposal of these effluents into the water can be toxic to living organisms (Lee *et al.*, 1999; Kadirvelu *et al.*, 2000). The biological activities are spoilt by the dyes in water bodies. They harm our health since they might induce cancer and mutagenesis. It is crucial to remove dyes from wastewater (Papic *et al.*, 2000; Kar *et al.*, 2021; Sivaraj *et al.*, 2001).

There are different types of methods to reduce dyes from industrial dye-contaminated wastewater such as precipitation (Zhu *et al.*, 2007), ion exchange, photocatalytic degradation (Yi *et al.*, 2018; Xu *et al.*, 2015; Yang *et al.*, 2018), biological oxidation (Manenti *et al.*, 2014; Ren *et al.*, 2018), adsorption (Fan *et al.*, 2016; He *et al.*, 2018), membrane filtration (Li *et al.*, 2017), electrochemical function coagulation, chemical oxidation, electro-dialysis, adsorption, a spectro-photometric method, liquid chromatography method, etc. The waste water purification from industries that are polluted with dye by photocatalysis has received a lot of interest recently. Advanced oxidation processes (AOPs), which produce electron-hole pair radicals capable of subsequent reactions are the technology behind photocatalytic degradation (Banerjee *et al.*, 2006).

In relation to purified polymer or ordinary composites (micro and macro composites), clay or nano clay filled polymer nanocomposites represent a new category of materials that have drawn significant attention for their excellent physical properties, including high dimensional stability, gas barrier performance, flame retardancy, and mechanical strength. Nanoclays are employed in nanocomposites owing to their natural abundance and extremely high form factor. Natural or fabricated clays are utilized as fillers in nanoplates. Kaolinite, Silhydrite, Smectite, Fluorohectorite, Zeolite, Sepiolite, Kenyaite, Saponite, Magadiite, Kanemite, Ilerite, and other natural and manufactured nanoclays are often employed as nanofiller in nanocomposite materials (Liu *et al.*, 2003; Lateef *et al.*, 2016). They often have crystalline shapes and a Nanometric thickness. The growing interest in ZnO as a prospective photocatalyst is being generated by its low cost and relative safety (Lu *et al.*, 2008; Sakthivel *et al.*, 2003; Hariharan *et al.*, 2006). However, several wurtzite-type ZnO properties result in several unavoidable drawbacks when utilized as photo-catalyst. As for example, ZnO can only demonstrate its photocatalytic ability when exposed to UV light. Its photocatalytic effectiveness is decreased as a consequence of quick recombination of photoexcited electron-hole pairs (Liu *et al.*, 2012; Lin *et al.*, 2009; Djurišić *et al.*, 2006). Additionally, the high crystal size and rapid growth rate of ZnO result in a low particular surface area, which prevents the catalyst from exposing enough active sites (Greene *et al.*, 2006; Greene *et al.*, 2003; Xu *et al.*, 2011). Numerous engineering techniques, including band structure engineering, micro/nano engineering, bionic engineering, co-catalyst engineering, surface/interface engineering, and others, have been established to address these problems (Xu *et al.*, 2011; Zhou *et al.*, 2007; Qin *et al.*, 2011; Li *et al.*, 2015). And it is discovered that this innovative approach and photocatalytic efficiency have been used widely in the domains of degrading organic contaminants (Zhou *et al.*, 2012; Linic *et al.*, 2011; Hu *et al.*, 2010; Yan *et al.*, 2015). Numerous ZnO matrix morphologies have been documented thus far, including nanospindles (Christopher *et al.*, 2011; Kuriakose *et al.*, 2014), nanoporous microds (Deng *et al.*, 2012), nanorods (Zheng *et al.*, 2007), nanoparticles, nano fibers (Xie *et al.*, 2010), microspheres (Lai *et al.*, 2010), nanosheets (Qin *et al.*, 2011). There is still plenty of room to increase the photo catalytic effectiveness because ZnO diameters range widely from tens to hundreds of nanometers. Since ZnO has a smaller size, its larger specified surface area exposes more effective sites.

The current work was aimed to remove the textile dye Eosin yellow from the environment for the benefit of the creatures. In the present study, a unique Mymensingh clay and ZnO composite (clay-ZnO) was prepared for the purpose of photocatalytic destruction of EY under UV and visible light.

MATERIALS AND METHODS:

Materials and Reagents

Mymensingh clay was a kind of gift from the Mymensingh local area. All studies utilized deioni-zed water that was acquired from a Millipore water purification device (Takashima Keiki Co Ltd. Japan). Zinc Acetate, Ammonium carbonate, EY, Na_2CO_3, $NaHCO_3$, Na_2SO_4, NaCl, $Ca(NO_3)_2.4H_2O$, $Zn(NO_3)_2$, $Al(NO_3)_3$, $Ba(NO_3)_2$ (Merck, Germany). All of the chemicals were of analytical grade and were utilized directly.

Preparation of clay-ZnO composite

In a 1000 mL beaker, the growth of the clay-ZnO composite photocatalyst was completed. The beaker was first filled with 500 mL of a 0.25M zinc acetate solution. The beaker then was charged with the necessary amounts of natural sources of clay (obtainned from Mymensingh); the clay was added to the prior solution to create a suspension, which was then heated to roughly 60 °C. After adding 250 mL of a 0.5M ammonium carbonate solution drop by drop

while agitating the suspension at a constant temperature of 60°C, zinc carbonate precipitated on the clay particle surfaces. Under experimental conditions, the suspension was aged for 2 hours to achieve total precipitation. Produced precipitates were filtered and washed with distilled water to remove contaminants. The precipitates were then dried for two hours in an oven set at 110°C. Finally, the samples of the produced composites were kept in a furnace for three hours at 600°C for calcinations (Qin *et al.*, 2011; Benkelberg and Warneck, 1995). The final, dry composite was crushed and sieved through sieves with a 140 mesh size before being placed in a desiccator for storage. The following reaction occurred in this scheme:

$$Zn(CH_3COO)_2+(NH_4)_2CO_3 \rightarrow ZnCO_3+2\ CH_3COONH_4$$

$$ZnCO_3 + Clay \rightarrow Clay\text{-}ZnO$$

Photocatalytic degradation study

Photocatalytic degradation capacity of Clay-ZnO composite was analyzed using EY as a refer-ence dye. 0.2 g of composite was kept in a beaker and charged into 100mL aqueous EY solution (2×10^{-5}M) under UV light (3.31×10^{-9} Ein cm^{-3} s^{-1}). The composites were separated by using centrifugal force. The excess concentration of EY was determined by UV-1650 PC, Shimadzu, Japan. The degradation capacity was monitored at discrete time interludes. The quantity of dye present in the clay-ZnO composite as flow served as the basis for calculating the rate of degradation.

$$\text{Degradation Ratio } (\%) = \frac{(Co-Ce)}{Co} \times 100\% \qquad (1)$$

Where, Co and Ce are the initial and equilibrated dye concentrations (mol/L).We also compared the degradation capacity in different ratio of clay-ZnO composite.

Characterization

A JEOL JSM-6400LA FESEM was employed to analyze the surface morphologies of ZnO, Mymensingh clay, and Clay-ZnO composites at a 5 kV accelerating voltage. An EDX spectrometer connected to the FESEM was utilized to determine the samples' elemental compositions. The infrared spectra were recorded on a SHIMADZU IR Tracer-100 infrared spectrophotometer in the region of 4000-400 cm^{-1}. The phase identification of the composites was censured by an XRD investigation carried out maintaining room temperature in the Ultima IV X-ray diffractometer. A UV-Vis spectrophotometer (UV-1650 PC, Shimadzu, Japan) was employed for the calculation of dye concentration.

RESULTS AND DISCUSSION:

Surface Morphology Analysis

The SEM images of clay, commercial ZnO, and composite in various ratios are represented in **Fig. 1(a)**, **1(b)**, and **1(c)** to **1(e)** with different magnification. The images suggest that the composite contains particles of different sizes. Clay particles appeared in different shapes, and since they collect randomly, the surface is heterogeneous. Contrarily, the particles of commercial ZnO are regularly shaped into various geometrical forms, including cubic, hexagonal, rhombic, etc. The surface is homogenous because of these regular shapes. Particle shapes in composites change based on how much clay and ZnO are included. Comparing composite particles to commercial ZnO and clay shows a different morphology. Particle size and shape change along with a rise in clay percentage of the composite. These particles aggregated, influencing the composite's surface's morphology. It should be beneficial for photocatalytic degradation since it enhances surface area (Waldemer and Tratnyek, 2006).

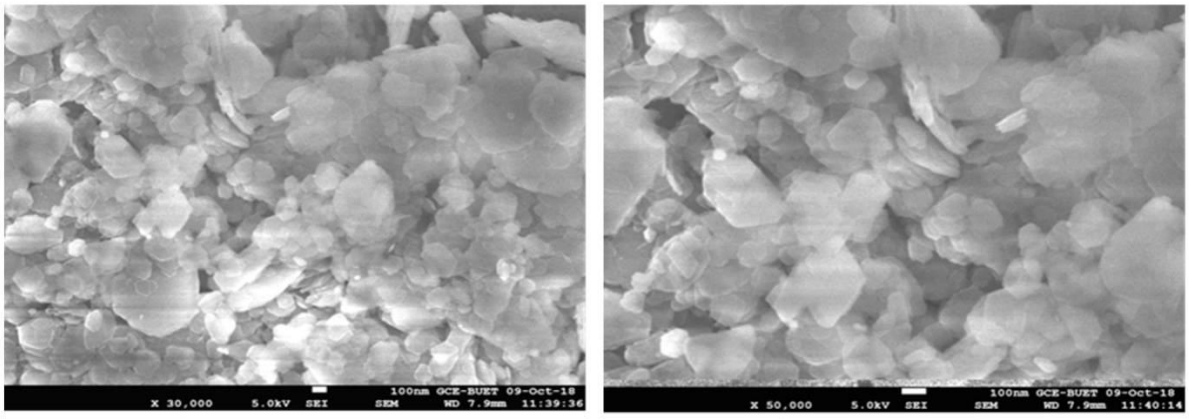

Fig. 1(a): SEM image of Mymensingh Clay.

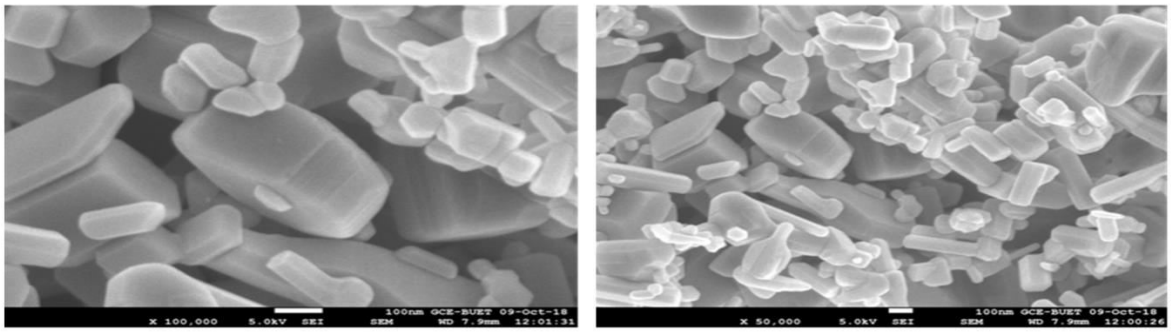

Fig. 1(b): SEM image of commercial ZnO.

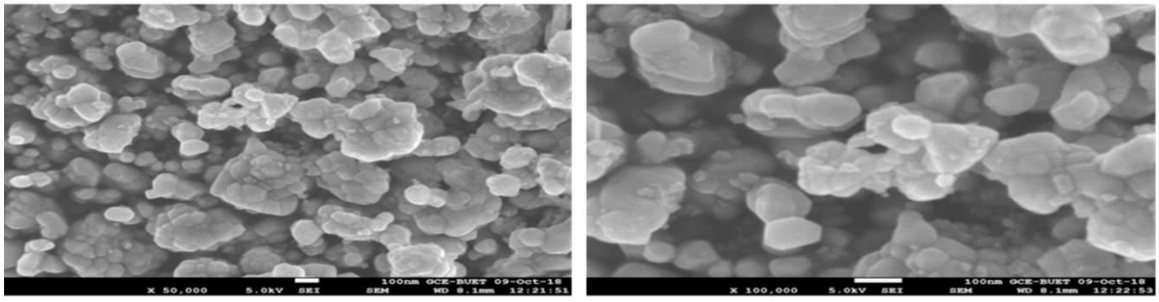

Fig. 1(c): SEM image of prepared composite (clay: ZnO; 12:88).

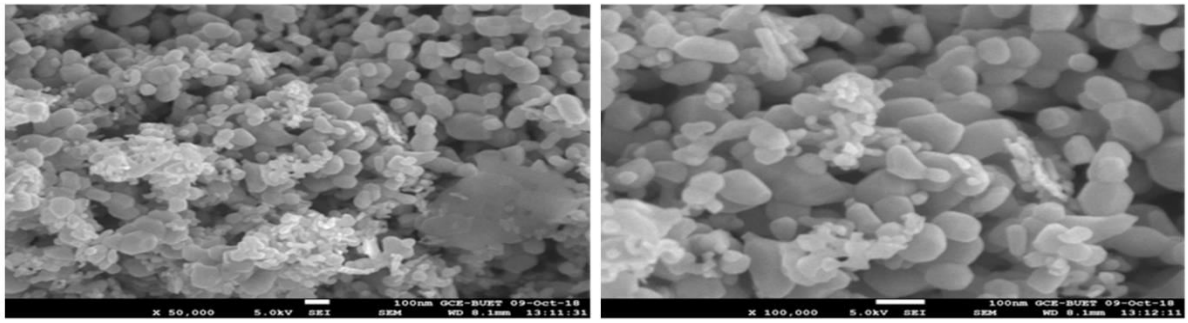

Fig. 1(d): SEM image of prepared composite (clay: ZnO; 25:75).

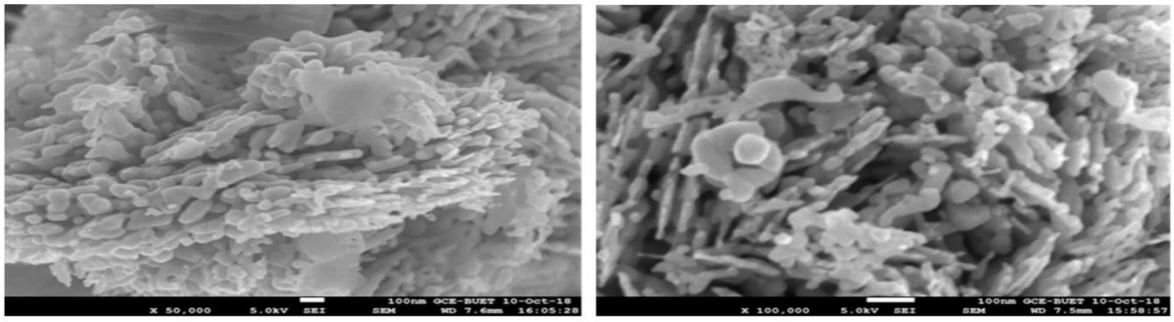

Fig. 1(e): SEM image of prepared composite (clay: ZnO; 50:50).

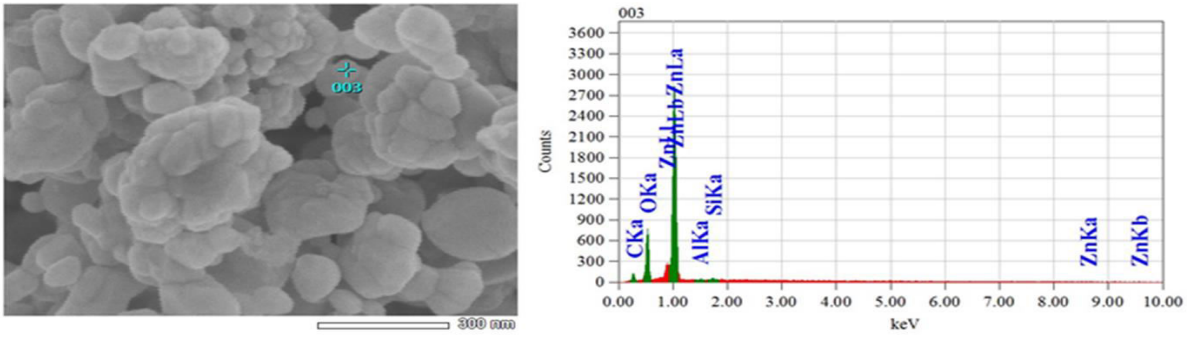

Fig. 2: EDX spectra of prepared composite (composition, clay to ZinO12:88).

XRD Analysis

The hexagonal phase of ZnO mentioned in JCPDS card No. 36-1451, with a = 0.3249 nm and c = 0.5206 nm, is the source of all the diffraction peaks in the XRD of commercial ZnO shown in **Fig. 3(a)**. There seem to be nine peaks at 2θ = 31.77˚, 34.42˚, 36.25˚, 47.53˚, 56.59˚, 62.85˚, 66.38˚, 67.94˚ and 69.09˚, which are (100), (002), (101), (102), (110), (103), (200), (112), and (201), respectively (Habib *et al.*, 2013). The sharpness of all the peaks indicates that these ZnO particles have such a high degree of crystallinity. The prepared composite's XRD, which is seen in **Fig. 3(b)**, contains all of the ZnO peaks, but their positions have indeed been slightly shifted, indicating that clay and ZnO have interacted at the molecular level. A composite's shifting crystal structure may influence the lattice parameter and, in effect, the surface morphology. Peaks for clay appear and get more intense as the content of clay in the composite increases, although the position has slightly shifted. Due to nearby peaks' influence, several peaks have been altered.

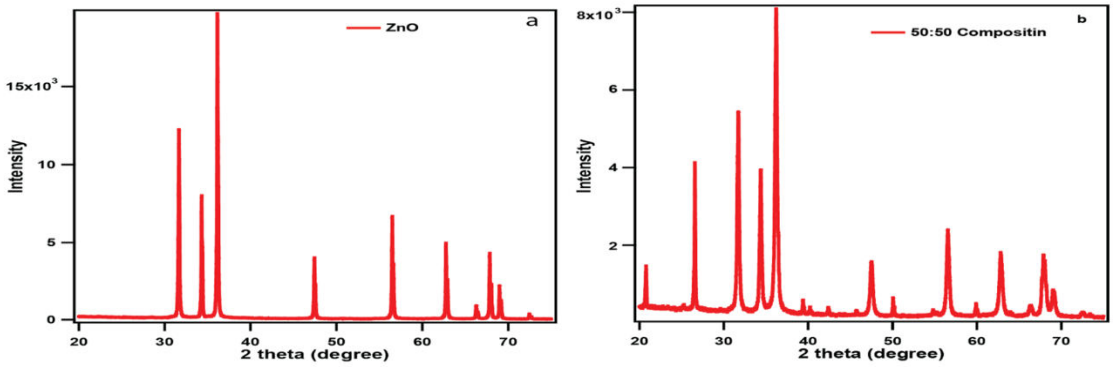

Fig. 3: XRD spectra of (a) ZnO and (b) composite of 50:50 compositions.

FTIR analysis

Fig. 4 presents the FT-IR spectra of commercial ZnO, prepared composites, and clay. It displays wide band characteristics below 1000 cm^{-1} that might be caused by overlapping Zn-O stretching (Viswanatha *et al.*, 2012; Gao *et al.*, 2003; Zuas and Hamim, 2013). The stretching bands of ZnO at 487.99 cm^{-1} and 437.84 cm^{-1} are overlapped, appearing in the bands at 495.71 and 439.77 cm^{-1}. The broad peak between in 3100 and 3600 cm^{-1} is assigned to the hydroxyl groups' fundamental stretching vibration (free or bonded) (Wickramasuriya *et al.*, 2021) which is further verified by the weak band at about 1620.21 cm^{-1} (Klingenberg and Vannice, 1996). The characteristics clay peak between 1000 and 500 cm^{-1} was observed. The peaks of the composite spectrum that was observed in clay and ZnO have undergone some modification. Few peaks at around 1100 $cm^{-1}$of the composite's spectrum seem to get more intense as the clay content increases, despite the fact that they are primarily remakes of the clay-specific peaks and have shifted positions. The peaks that indicate ZnO is present in the prepared composite do not appear to have altered significantly. It may be because ZnO predominates over clay in the prepared composites. The vibrations of atmospheric CO_2 might be accountable for a faint band at about 2400 cm^{-1}. **Fig. 2's** composite EDX analysis shows that the main components of the prepared composite were clay and ZnO. No other peaks for impurities were observed in the spectrum of composite. So, the prepared composite samples are in pure state.

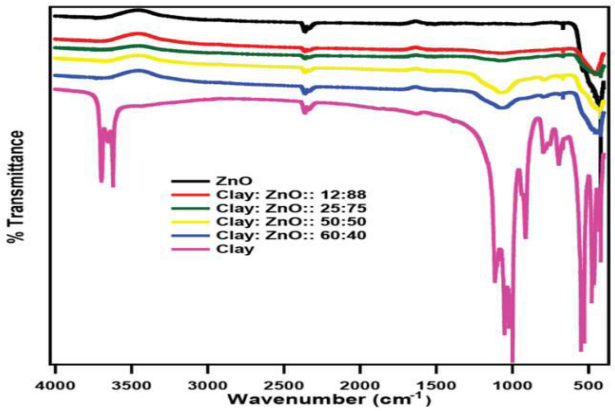

Fig. 4: FTIR spectra of clay, ZnO and prepared clay-ZnO composite of different compositions, respectively.

Effect of composition of prepared Clay-ZnO composite on photodegradation

The efficient clay-ZnO composition for the composite was determined by carrying out illumination experiments using 0.20 g composite of different clay-ZnO ratios, 2.0×10^{-5} M concentration of EY with the light intensity of 3.31×10^{-9} Ein cm^{-3} s^{-1}. The

blank experiment was conducted using 0.20 g of pure ZnO with the same experimental condition to figure out the composition effect as illustrated in **Fig. 5**. Based on the observations, 25:75 Clay-ZnO composite displayed photocatalytic degradation efficiency of 44%. Illumination generates electrons and holes in ZnO and these electrons and holes create secondary species/radicals that cause photo degradation. Now, effective electron and hole separation elongates the charge carrier's lifetime and improves the adsorption of interfacial charge transfer of substrates (Serpone *et al.*, 1995). In the composites, electrons, and holes separation are efficient owing to mixing of clay with ZnO as it helps to delay the recombination process of the charges. Therefore, the photocatalytic activity is relied on the quantity of clay and ZnO in the developed composite that helps to separate the charges efficiently, ultimately enhancing the production of secondary species/radicals (Habib *et al.*, 2013). Optimization was seen at the composition of clay to ZnO at 25:75 which gives the maximum photo degradation of EY nearly 45%. An increase in the composite com-position causes ZnO particles to accumulate on the clay's surface, and it seems that the ZnO particles are trapping the clay. At this stage, a composite mostly made of ZnO acts exactly like pure ZnO.

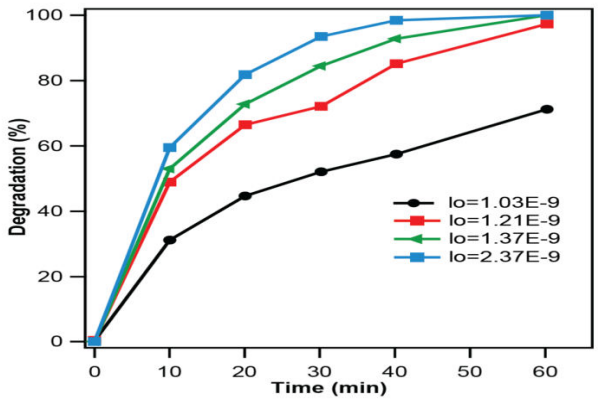

Fig. 5: Changes in the percentage of EY solution degradation with changes in the clay-ZnO ratio for the composite at various times under UV irradiation using 2.0×10^{-5} M EY and light intensity of 3.31×10^{-9} Ein cm^{-3} s^{-1}.

Effect of prepared composite amount

Photo degradation experiment was performed using different composite amount varying from 0.1 to 0.5 g in 100 mL solution keeping EY concentration of 2.0×10^{-5} M and intensity of UV light of 3.31×10^{-9} Ein cm^{-3} s^{-1} constant as shown in **Fig. 6**. It is found that photo degradation efficiency increases with the increase of the composite amount from 0.1 g to 0.35 g, gives maximum efficiency at 0.35 g then degradation efficiency decreases with the increase of composite amount. The catalyst's surface has excessive active sites due to an increase in composite quantity, which promotes the initial increase in degradation efficiency (Habib *et al.*, 2013). Whereas, the degradation efficiency decreases with the increase of composite amount is because the excessive composite amount causes the hindrance and blocking of light penetration to the catalyst surface (Kim and Park, 2006). Additionally, particle aggregation is significant at higher amounts of composite, thereby reduces the number of active sites on the catalyst surface. Therefore, the degradation efficiency reaches its maximum at 0.35 g of composite amount then decreases with further increase of the composite amount.

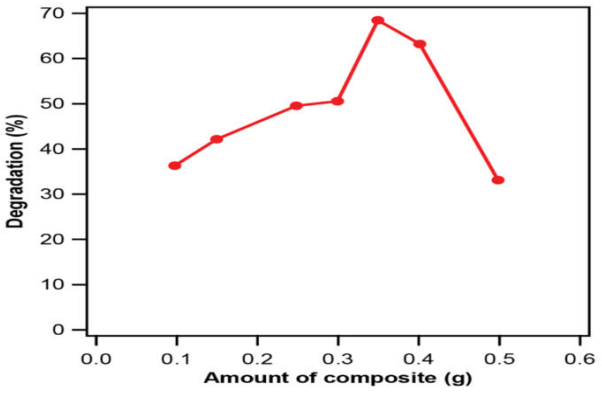

Fig. 6: Change of the degradation percentage of EY solution with the change of the composite in UV irradiation using 2.0×10^{-5} M concentration of EY with light intensity of 3.31×10^{-9} Ein cm^{-3} s^{-1}.

Effect of primary concentration of EY

As shown in **Fig.7**, the photo degradation efficiency was originated as a function of primary concentration of EY. The photo degradation efficiency was lowered with increasing EY concentration without any distinct pattern or obeying any mathematical equation. No evidence was found that this photo degradation process goes through chain mechanism, therefore, only a constant amount of oxidizing species is generated from the constant amount of catalyst that oxidizes a certain amount of dye molecules. As a result, a fixed quantity of catalyst at constant light intensity can oxidize only a certain amount of dye molecules at a period and that cannot be altered with increasing the quantity of dye molecule. Since, the photo degradation efficiency (percentage of degradation) is calculated with decrease in dye con-

centration with respect to primary dye concentration, that justifies why degradation efficiency decreases with increasing initial dye concentration. Additionally, a dye solution with a high concentration can block light from reaching the rest of the solution. Higher concentration hence resulted in decreased photo degradation efficiency.

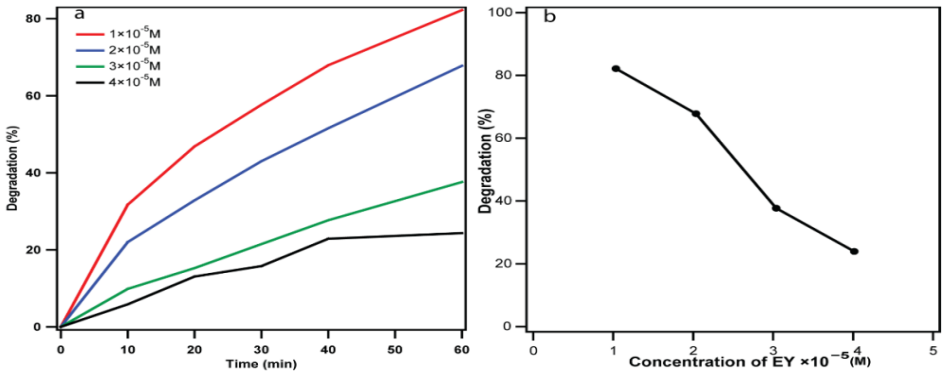

Fig. 7: Change of the degradation percentage of EY at (a) different time for different concentration (b) change of initial dye concentration in UV irradiation with light intensity of 3.31×10^{-9} Ein cm^{-3} s^{-1}.

Effect of discrete light sources

Fig. 8 exhibits the utilization of UV light having an intensity of 3.31×10^{-9} Ein cm^{-3} s^{-1} and visible light to observe the impacts of various light sources. In this instance, the optimum EY concentration was 1.00×10^{-5} M, and the composite weight was 0.35 g. By introducing the dye to UV radiation, the maximum rate of degradation of EY about 82.2% was observed. The degradation between the light sources for visible light is less significant, at around 63%. It is generally known that when the wavelength of the light source is reduced, an increase in the formation of electron-hole pairs occurs. UV light will therefore be more efficient than visible light for lights of equal intensity.

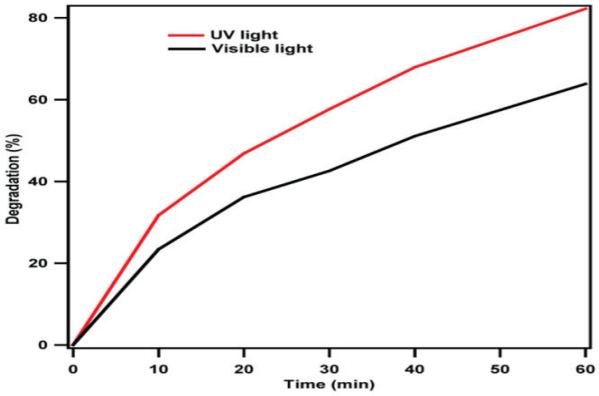

Fig. 8: Variation of degradation percentage of $1.00x10^{-5}$ M EY solution under various light sources.

Effect of light intensity

Presented in **Fig. 9** is alteration in the photo degraded percentage of EY with time for various light intensity indicating that the degradation of EY enhanced with increasing light intensity and complete degradation occurred within 1 hour at the light intensity of or above 1.21×10^{-9} Ein cm^{-3} s^{-1}. The proposed photo degradation of EY mechanism said that the quantity of charged particles (electrons and holes) generated from composite are dependent on the quantity of photons entering into composite surface. Therefore, the generation of $OH^{\bullet}$ radicals and other reactive species that oxidize dye molecule are dependent on number of photons and light intensity. This mechanism explains with experimental observation for increased photo degradation efficiency with increasing light intensity. It was noticed that to reach complete dye degradation as the light intensity increases from 1.03×10^{-9} to 1.36×10^{-9} Ein cm^{-3} s^{-1}. Even though, experiments were carried out using light intensity higher than 1.36×10^{-9} Ein cm^{-3} s^{-1} but no experiment was possible to carry out at light intensity below 1.03×10^{-9} Ein cm^{-3} s^{-1} due to laboratory limitations.

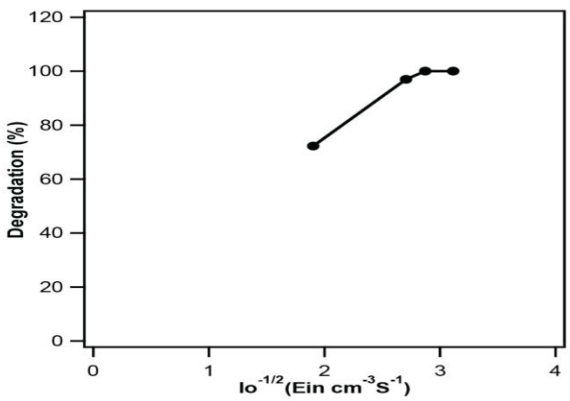

Fig. 9: Change of the percentage of degradation of EY solution with the change of light intensity at different time using 2.0×10^{-5} M concentration of EY.

Therefore, no real trend that photo degradation of EY follow with light intensity was figured out using data from only three different light intensity experiments. Nevertheless, attempts were made to figure out a relationship of light intensity with photo degradation efficiency using the data acquired from the light intensity experiments that yielded photo degradation below 100 percent.

Effect of cations and anions

Fig. 10 illustrates the findings of the study on the effects of cation and anion using a composite of 0.35 g and 1.00×10^{-5} M EY solution. Investigated were the effects of Ca^{2+}, Zn^{2+}, Ba^{2+}, and Al^{3+} cations on photodegradation. In comparison to other cations, the Zn^{2+} ion among them appears to accelerate photodegradation of EY. It could be because of its significant reduction potential and effective adsorption onto the composite's surface. Utilizing sodium salts of HCO_3^-, CO_3^{2-}, Cl^-, NO_3^-, and SO_4^{2-}, the effect of anion was studied. All of these have reduced the degradation percentage. These ions decrease poto degradation by scavenging the most reactive hydroxide radicals (Islam *et al.*, 2010).

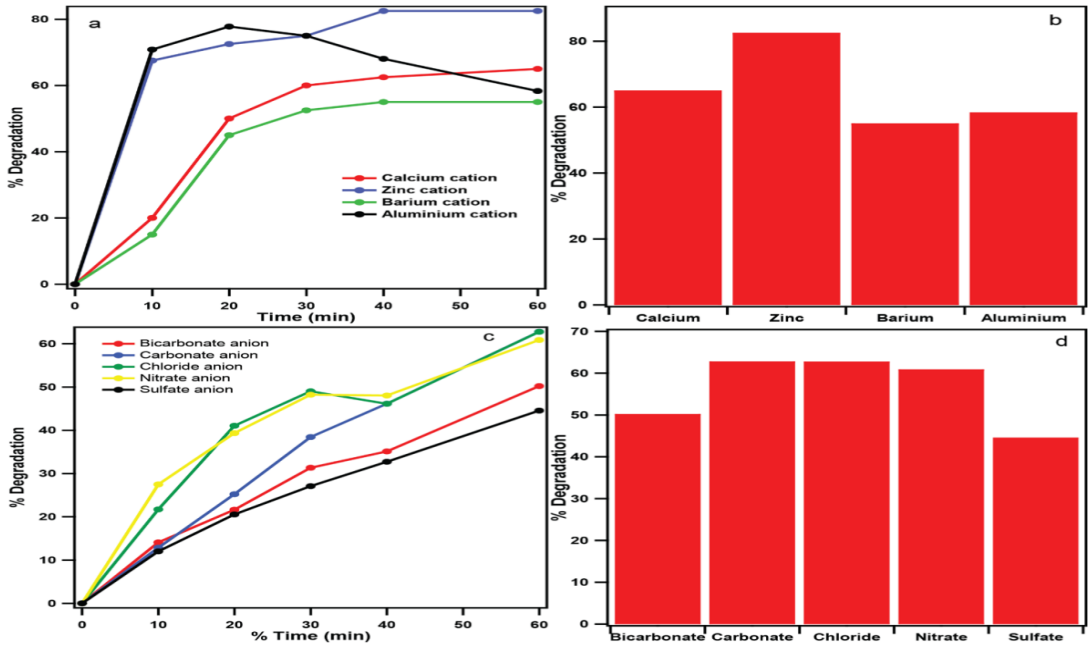

Fig. 10: (a) Effect of cations on Photodegradation process, (b) Photodegradation in presence of different cations at 60 minutes, (c) Effect of anions on Photodegradation process, (d) Photodegradation in presence of different anions at 60 minutes.

CONCLUSION:

In the present study, we here report the effective synthesis of clay-ZnO composite photo-catalysts with varying clay and ZnO compositions ranging from 12:88 to 50:50. The interpretation of the clay-ZnO composites by SEM, EDX, FTIR, and XRD has been beneficial. The material with the composition clay: ZnO had the highest % removal of EY, which includes adsorption and photo catalytic degradation (25:75). When 1.0×10^{-5} M EY was exposed to irradiation for 1 hour while contained in 3.5 g/L of composite suspension, about 82.21% degradation of EY was seen. The photo catalytic degradation of EY was evident to be adversely affected by the consequences of several anions, including HCO_3^-, CO_3^{2-}, Cl^-, NO_3^-, and SO_4^{2-}. On the contrary, the addition of Zn^{2+} accelerated EY degradation rate. Photodegradation was observed to be at its highest using UV light, but visible light showed less photodegradation. A strong UV radiation causes total degradation. Since all these samples are expected to quickly absorb the organic dyes during the continuous flow of effluents into the river and can be applied as an efficacious photocatalyst substitute to treat wastewater containing dyes, it could be concluded that the typical prepared composites should be very important in the industrialized era. Additionally, this composite is simple to make from inexpensive clay, making the procedure economical. The method is environmentally friendly since the photocatalyst is recycled.

ACKNOWLEDGEMENT:

The authors are thankful to the Committee for Advanced Studies and Research (CASR), BUET,

Bangladesh and Ministry of Science and Technology, People's Republic of Bangladesh for funding.

CONFLICTS OF INTEREST:

The authors declare that they have no conflict of interests.

REFERENCES:

1) Alqadami AA, Naushad M, Abdalla MA, (2016). Adsorptive removal of toxic dye using Fe_3O_4-TSC nanocomposite: Equilibrium, kinetic, and thermodynamic studies. *J Chem Eng Data*, **61**(11), 3806–3813. https://doi.org/10.1021/acs.jced.6b00446
2) Banerjee S, Gopal J, Muraleedharan P, (2006). Physics and chemistry of photocatalytic titanium dioxide: Visualization of bactericidal activity using atomic force microscopy. *Curr Sci*, **90**(25), 1378–1383. https://www.jstor.org/stable/24091987
3) Benkelberg HJ, Warneck P, (1995). Photodecomposition of iron(III) hydroxo and sulfato complexes in aqueous solution: Wavelength dependence of OH and 804- quantum yields. *J Phys* Chem, **99**, 5214–5221. https://doi.org/10.1021/J100014A049
4) Christopher P, Xin H, Linic S. (2011). Visible-light-enhanced catalytic oxidation reactions on plasmonic silver nanostructures. *Nat Chem*, **3**, 467–472. http://dx.doi.org/10.1038/nchem.1032
5) Deng Q, Duan X, Ng DHL, (2012). Ag nanoparticle decorated nanoporous ZnO microrods and their enhanced photocatalytic activities. *ACS Appl Mater Interfaces*, **4**, 6030-6037. https://doi.org/10.1021/am301682g
6) Djurišić AB, Leung YH, (2006). Optical properties of ZnO nanostructures. *Small*, **2**, 944-961. http://dx.doi.org/10.1002/smll.200600134
7) Fan S, Tang J, Wang Y, (2016), Biochar prepared from co-pyrolysis of municipal sewage sludge and tea waste for the adsorption of methylene blue from aqueous solutions: Kinetics, isotherm, thermodynamic and mechanism. *J Mol Liq*, **220**, 432–441. http://dx.doi.org/10.1016/j.molliq.2016.04.107
8) Gao Y, Masuda Y, Peng Z, (2003). Room temperature deposition of a TiO_2 thin film from aqueous peroxotitanate solution. *J Mater Chem*, **13**, 608–613. https://doi.org/10.1039/B208681F
9) Greene LE, Law M, Goldberger J, (2003). Low-temperature wafer-scale production of ZnO nanowire arrays. *Angew Chemie - Int Ed*, **42**(26), 3031–3034. https://doi.org/10.1002/anie.200351461
10) Greene LE, Yuhas BD, Law M, (2006). Solution-grown zinc oxide nanowires. *Inorg* Chem, **45**, 7535–7543. https://doi.org/10.1021/ic0601900
11) Habib MA, Shahadat MT, Bahadur NM, (2013). Synthesis and characterization of ZnO-TiO_2 nanocomposites and their application as photocatalysts. *Int Nano Lett*, **3**, 1–8. https://doi.org/10.1186/2228-5326-3-5
12) Hariharan C, (2006). Photocatalytic degradation of organic contaminants in water by ZnO nanoparticles: Revisited. *Appl Catal A Gen*, **304**(10), 55–61. https://doi.org/10.1016/j.apcata.2006.02.020
13) He K, Zeng Z, Chen A, (2018). Advancement of Ag–Graphene Based Nanocomposites: An Overview of Synthesis and Its Applications. *Small*, **14**(32), 1–13. https://doi.org/10.1002/smll.201800871
14) Hu C, Peng T, Hu X, (2010). Plasmon-induced photodegradation of toxic pollutants with Ag-AgI/Al_2O_3 under visible-light irradiation. *J Am Chem Soc*, **132**, 857–862. https://doi.org/10.1021/ja907792d
15) Islam MS, Hossain MM, Islam TS, (2010). Effect of pH , Ions and Ionic Strength on TiO_2-mediated photodegradation of Brilliant Orange. *Dhaka Univ J Sci*, **58**, 187–190. https://www.banglajol.info/index.php/DUJS
16) Kadirvelu K, Faur-Brasquet C, Le Cloirec P, (2000). Removal of Cu(II), Pb(II), and Ni(II) by adsorption onto activated carbon cloths. *Langmuir*, **16**(22), 8404–8409. https://doi.org/10.1021/la0004810
17) Kar K, Hossain MA, and Roshni A. (2021). Recovery and recycling of valuable metals from low-grade ores using microorganisms: a brief review. *Am. J. Pure Appl. Sci*., **3**(1), 1-16. https://doi.org/10.34104/ajpab.021.01016
18) Kim DS, Park YS, (2006). Photocatalytic decolorization of rhodamine B by immobilized TiO_2 onto silicone sealant. *Chem Eng J*, **116**, 133-137. https://doi.org/10.1016/j.cej.2005.10.013
19) Klingenberg B, Vannice MA, (1996). Influence of pretreatment on lanthanum nitrate, carbonate, and oxide powders. *Chem Mater*, **8**,

2755-2768.
https://doi.org/10.1021/cm9602555

20) Kuriakose S, Choudhary V, Satpati B, (2014). Facile synthesis of Ag-ZnO hybrid nanospindles for highly efficient photocatalytic degradation of methyl orange. *Phys Chem Chem Phys*, **16**, 17560–17568. http://dx.doi.org/10.1039/C4CP02228A
21) Lai Y, Meng M, Yu Y, (2010). One-step synthesis, characterizations and mechanistic study of nanosheets-constructed fluffy ZnO and Ag/ZnO spheres used for Rhodamine B photodegradation. *Appl Catal B Environ*, **100**, 491–501. http://dx.doi.org/10.1016/j.apcatb.2010.08.027
22) Lateef A, Nazir R, Jamil N, (2016). Synthesis and characterization of zeolite based nanocomposite: An environment friendly slow release fertilizer. *Microporous Mesoporous Mater*, **232**, 174–183. http://dx.doi.org/10.1016/j.micromeso.2016.06.020
23) Lee CK, Low KS, Gan PY, (1999). Removal of some organic dyes by acid-treated spent bleaching earth. *Environ Technol (United Kingdom)*, **20**(1), 99–104. https://doi.org/10.1080/09593332008616798
24) Linic S, Christopher P, Ingram DB. (2011). Plasmonic-metal nanostructures for efficient conversion of solar to chemical energy. *Nat Mater*, **10**, 911–921. http://dx.doi.org/10.1038/nmat3151
25) Lin D, Wu H, Zhang R, (2009). Enhanced photocatalysis of electrospun Ag-ZnO heterostructured nanofibers. *Che Mater*, **21**(15), 3479-3484. https://doi.org/10.1021/cm900225p
26) Li Q, Li Y, Ma X, (2017). Filtration and adsorption properties of porous calcium alginate membrane for methylene blue removal from water. *Chem Eng J*, **316**, 623–630. https://www.sciencedirect.com/science/article/pii/S1385894717301080
27) Liu HR, Shao GX, Zhao JF, (2012). Worm-like Ag/ZnO core-shell heterostructural composites: Fabrication, characterization, and photocatalysis. *J Phys Chem C*, **116**(30), 16182-16190. https://doi.org/10.1021/jp2115143
28) Liu T, Lim KP, Tjiu WC, (2003). Preparation and characterization of nylon 11/organoclay nanocomposites. *Polymer*, **44**(12), 3529-3535. https://doi.org/10.1016/S0032-3861(03)00252-0
29) Lu F, Cai W, Zhang Y.(2008). ZnO hierarchical micro/ nanoarchitectures: Solvo-thermal synthesis and structurally enhanced photocatalytic performance. *Adv Funct Mater*, **18** (7), 1047–1056. https://doi.org/10.1002/adfm.200700973
30) Li X, Yu J, and Low J, (2015). Engineering heterogeneous semiconductors for solar water splitting. *J Mater Chem A*, **3**, 2485–2534. http://dx.doi.org/10.1039/C4TA04461D
31) Manenti DR, Módenes AN, Soares PA, (2014). Assessment of a multistage system based on electrocoagulation, solar photo-Fenton and biological oxidation processes for real textile wastewater treatment. *Chem Eng J*, **252**, 120–130. http://dx.doi.org/10.1016/j.cej.2014.04.096
32) Nasr MF, Abo El-Ola SM, Ramadan A, (2006). A comparative study between the adsorption behavior of activated carbon fiber and modified alginate I. Basic dyes adsorption. *Polym - Plast Technol* Eng, **45**(3), 335–340. http://dx.doi.org/10.1080/03602550600553176
33) Niazai S, Rahimzai AA, Danesh M, and Safi B. (2022). Numerical solution of diffusion equation with caputo time fractional derivatives using finite-difference method with Neumann and Robin boundary conditions, *Int. J. Mat. Math. Sci*., **4**(1), 01-14. https://doi.org/10.34104/ijmms.022.010014
34) Papic S, Koprivanac N, Metes A, (2000). Optimizing polymer-induced flocculation process to remove reactive dyes from wastewater. *Environ Technol (UK)*, **21**(1), 97–105. https://doi.org/10.1080/09593332108618143
35) Qin H, Li W, Xia Y, (2011). Photocatalytic activity of heterostructures based on ZnO and N-doped ZnO. *ACS Appl Mater Interfaces*, **3**(8), 3152–3156. https://doi.org/10.1021/am200655h
36) Ren X, Zeng G, Tang L, (2018). Effect of exogenous carbonaceous materials on the bioavailability of organic pollutants and their ecological risks. *Soil Biol Bioche*, **116**, 70-81. http://dx.doi.org/10.1016/j.soilbio.2017.09.027
37) Sakthivel S, *et al*. (2003). Solar photocatalytic degradation of azo dye: Comparison of photocatalytic efficiency of ZnO and TiO_2. *Sol Energy Mater Sol Cells*, **77**(1), 65–82. https://doi.org/10.1016/S0927-0248(02)00255-6
38) Samadder R, Akter N, Roy AC, (2020). Magnetic nanocomposite based on polyacrylic acid

and carboxylated cellulose nanocrystal for the removal of cationic dye. *RSC* Adv, **10**, 11945–11956. https://doi.org/10.1039/D0RA00604A

39) Serpone N, Maruthamuthu P, Pichat P, (1995). Exploiting the interparticle electron transfer process in the photocatalysed oxidation of phenol, 2-chlorophenol and pentachloro-phenol: chemical evidence for electron and hole transfer between coupled semiconductors. *J Photochem Photobiol A Chem*, **85**, 247–255. https://doi.org/10.1016/1010-6030(94)03906-B
40) Sivaraj R, Namasivayam C, Kadirvelu K, (2001). Orange peel as an adsorbent in the removal of Acid violet 17 (acid dye) from aqueous solutions. *Was Mana*, **21**(1), 105–110. https://doi.org/10.1016/S0956-053X(00)00076-3
41) Viswanatha R, Venkatesh TG, Vidyasagar CC, (2012). Preparation and Characterization of ZnO and Mg-ZnO nanoparticle. *Arch Appl Sci Res*, **4**, 480–486.
42) Waldemer RH, Tratnyek PG, (2006). Kinetics of contaminant degradation by permanganate. *Environ Sci Technol*, **40**, 1055–1061. https://doi.org/10.1021/es051330s
43) Wickramasuriya AIR, Arachchige RCW, Kottegoda IRM, (2021). Characterization and Modification of Clay for Removal of Drinking Water Hardness. *Mater Sci Res India*, **18**, 318–331. https://doi.org/10.13005/msri/180307
44) Xie J, Wu Q. (2010). One-pot synthesis of ZnO/Ag nanospheres with enhanced photocatalytic activity. *Mater Lett*, **64**, 389–392. http://dx.doi.org/10.1016/j.matlet.2009.11.026
45) Xu D, Cheng B, Cao S, (2015). Enhanced photocatalytic activity and stability of Z-scheme Ag_2CrO_4-GO composite photocatalysts for organic pollutant degradation. *Appl Catal B Environ*, **164**, 380–388. https://doi.org/10.1016/j.apcatb.2014.09.051
46) Xu S, Wang ZL. (2011). One-dimensional ZnO nanostructures: Solution growth and functional properties. *Nano Res*, **4**, 1013–1098. https://doi.org/10.1007/s12274-011-0160-7
47) Xu T, Zhang L, Cheng H, (2011). Significantly enhanced photocatalytic performance of ZnO via graphene hybridization and the mechanism study. *Appl Catal Envi*, **101**, 382-387. http://dx.doi.org/10.1016/j.apcatb.2010.10.007
48) Yan X, Wang X, Gu W, (2015). Single-crystalline $AgIn(MoO_4)_2$ nanosheets grafted Ag/AgBr composites with enhanced plasmonic photocatalytic activity for degradation of tetracycline under visible light. *Appl Catal B Environ*, **164**, 297–304. https://doi.org/10.1016/j.apcatb.2014.09.046
49) Yang Y, Zhang C, Lai C, (2018). BiOX (X = Cl, Br, I) photocatalytic nanomaterials: Applications for fuels and environmental management. *Adv Colloid Interface Sci*, **254**, 76–93. https://doi.org/10.1016/j.cis.2018.03.004
50) Yi H, Huang D, Qin L, (2018). Selective prepared carbon nanomaterials for advanced photocatalytic application in environmental pollutant treatment and hydrogen production. *Appl Catal B Environ*, **239**(30), 408–424. https://doi.org/10.1016/j.apcatb.2018.07.068
51) Zheng Y, *et al*. (2007). Ag/ZnO heterostructure nanocrystals: Synthesis, chara-cterization, and photocatalysis. *Inorg Chem*, **46**, 6980–6986. https://doi.org/10.1021/ic700688f
52) Zhou G, Deng J, (2007). Preparation and photocatalytic performance of Ag/ZnO nanocomposites. *Mater Sci Semi Process*, **10**, 90-96. https://doi.org/10.1016/j.mssp.2007.05.003
53) Zhou X, Liu G, Yu J, (2012). Surface plasmon resonance-mediated photocatalysis by noble metal-based composites under visible light. *J Mater Chem*, **22**, 21337-21354. https://doi.org/10.1039/C2JM31902K
54) Zhu MX, Lee L, Wang HH, (2007). Removal of an anionic dye by adsorption/precipitation processes using alkaline white mud. *J Hazard Mater*, **149**(3), 735-741. https://doi.org/10.1016/j.jhazmat.2007.04.037
55) Zuas O, Hamim N, (2013). Synthesis, characterization and properties of CeO_2-doped TiO_2 composite nanocrystals. *Medziagoty*, **19**, 443-447. https://doi.org/10.5755/j01.ms.19.4.2732

Citation: Halder D, Islam MN, Hossain MM, Rahman MA, Samadder R, and Rahman MM. (2022). Synthesis a clay based photocatalyst for the removal of eosin yellow in aqueous solution, *Int. J. Mat. Math. Sci.*, **4**(4), 83-93. https://doi.org/10.34104/ijmms.022.083093